A Method for Calculating Reliable Supersaturation Reveals Low Values in Tropical Rainy-Season Clouds

DAVID M. ROMPS[a,b]

[a] *Department of Earth and Planetary Science, University of California, Berkeley, California*
[b] *Climate and Ecosystem Sciences Division, Lawrence Berkeley National Laboratory, Berkeley, California*

(Manuscript received 25 November 2024, in final form 13 March 2025, accepted 24 April 2025)

ABSTRACT: High supersaturation on the order of 10% in unpolluted moist convection is a prerequisite for substantial warm-phase aerosol invigoration. However, such high supersaturation has not yet been confidently observed. To accurately detect high supersaturation, the analysis method must avoid generating spuriously high values, and one such method is presented here. Applied to aircraft data from GoAmazon's relatively unpolluted rainy season, the method finds only low supersaturation: the observed values have a median of 0.5% and are all less than about 1%. Combining both rainy-season and dry-season measurements, the convective supersaturation during GoAmazon is found to scale as the boundary-layer aerosol concentration to the −2/3 power, as previously predicted. For moist convection of any type, a 10% supersaturation would require a very high vertical velocity, a very low sum of droplet diameters per volume, or some high/low combination of both.

KEYWORDS: Convective-scale processes; In situ atmospheric observations; Aerosol-cloud interaction

1. Introduction

A popular hypothesis is that higher aerosol concentrations directly invigorate convection, i.e., that air pollution increases the vertical velocities in moist convective updrafts through its effect on microphysics (Stier et al. 2024). Although the existence of this aerosol invigoration remains unsettled as an empirical matter (Varble et al. 2023), three theories have been proposed for how it might work: the humidity–entrainment, cold-phase, and warm-phase mechanisms.

In the proposed humidity–entrainment mechanism (Abbott and Cronin 2021), aerosols inhibit precipitation, leading to more moistening of the environment, which reduces the impact of entrainment on subsequent updrafts, leading to higher bouyancies and higher updraft speeds. So far, this has only been demonstrated in domains coupled to a weak temperature gradient (WTG) approximation for large-scale motion (Sobel and Bretherton 2000; Raymond and Zeng 2005), prompting concerns about its generality (Dagan et al. 2022). In the proposed cold-phase mechanism (Rosenfeld et al. 2008), aerosols inhibit precipitation, leading to more lofting of liquid to altitudes where it freezes, increasing the latent heating from freezing, leading to higher buoyancies and higher updraft speeds. The plausibility of this mechanism has been called into question on the grounds that it assumes rapid freezing and fallout of condensates (Igel and van den Heever 2021) and the absence of entrainment (Peters et al. 2023); relaxing either of those assumptions tends to greatly reduce or reverse the effect (Igel and van den Heever 2021; Peters et al. 2023).

The third theory, and the topic of study here, is the warm-phase mechanism (Koren et al. 2014; Seiki and Nakajima 2014; Saleeby et al. 2015; Sheffield et al. 2015; Fan et al. 2018; Cotton and Walko 2021). In this mechanism, aerosols lower the supersaturation in cloudy updrafts, hastening the release of latent heat, leading to higher buoyancies and higher updraft speeds. Substantial warm-phase invigoration requires the typical supersaturation in unpolluted cloudy updrafts to be on the order of 10% (Igel and van den Heever 2021; Romps et al. 2023), but all in situ measurements of supersaturation in cloudy updrafts (all made using the quasi-steady approximation described in the next section) have found median values in the range of ∼0.1%–0.3% (Warner 1968; Politovich and Cooper 1988; Prabha et al. 2011; Siebert and Shaw 2017; Romps et al. 2023). Consistent with this absence of evidence for high supersaturation, observations show no evidence of a correlation between aerosol concentrations and warm-phase updraft speeds (Öktem et al. 2023).

On the other hand, previous measurements of supersaturation have all been in continental conditions, such as over Australia (Warner 1968), the United States (Politovich and Cooper 1988), India (Prabha et al. 2011), the Netherlands (Siebert and Shaw 2017), and the Amazon during the dry season (Romps et al. 2023). As a result, previous observations did not have the low background concentrations of aerosols that might tend to favor high supersaturation. To extrapolate to low aerosol conditions, Romps et al. (2023) proposed that the supersaturation should scale, all else equal, as the aerosol concentration to the −2/3 power. According to this theory, boundary-layer aerosol concentrations as low as 100 cm^{-3} would give supersaturation values in moderately fast updrafts (∼1–10 $m\ s^{-1}$) only on the order of 1%.

Here, we present in situ measurements of supersaturation in cloudy updrafts over the Amazon during the rainy season, which is a location and time when warm-phase invigoration has been proposed to be operating (Fan et al. 2018). The boundary-layer aerosol concentrations are substantially lower during the rainy season compared to the dry season, raising the prospect, checked here, that the supersaturation might be

Corresponding author: David M. Romps, romps@berkeley.edu

DOI: 10.1175/JAS-D-24-0265.1

large. Using in situ data from both the rainy season and dry season, we also evaluate the −2/3 power-law scaling proposed by Romps et al. (2023).

Throughout most of this manuscript, we will focus on relatively steady ascending motion made possible by latent heating. This focus is motivated by the fact that such motion is responsible for most tropical precipitation (Schumacher and Houze 2003; Schumacher and Funk 2023), it attains the highest buoyancies and vertical velocities, it is the focus of studies on aerosol invigoration (e.g., Fan et al. 2018), and its supersaturation can be estimated using the quasi-steady approximation, as discussed in the next section. All other ascending motion sampled by the aircraft is associated with eddies in which the latent heating is zero, incipient, or ancillary. As a shorthand, we will henceforth use "moist-convective updrafts" or simply "updrafts" to refer to steady ascending motion made possible by latent heating.

2. Theory

The supersaturation S is defined as $S = p_v/p_v^* - 1$, where p_v is the partial pressure of water vapor and $p_v^* = p_v^*(T)$ is the saturation vapor pressure at the temperature T of the air parcel. Standard aircraft instruments are unable to measure supersaturation directly because they do not operate well in the presence of liquid water and are not able to measure p_v and T to the needed accuracy (Korolev and Mazin 2003; Fujiwara et al. 2003; Shen et al. 2018; Yeom et al. 2019). Even the advanced infrared absorption hygrometer of Ditas et al. (2012) is only able to measure p_v to within a few percent. Alternatively, however, we may estimate the supersaturation in cloud updrafts using the quasi-steady approximation (Squires 1952).

A natural way to define the quasi-steady approximation is as $dS/dt = 0$. To simplify the derivations, it is standard practice to derive an expression that is accurate to first order in S and first order in p_v/p, which is justifiable so long as $S \ll 1$ (i.e., $S \ll 100\%$) and $p_v/p \ll 1$. At that level of approximation, we can write $S = q_v/q_v^* - 1$, where q_v is the mass fraction of water vapor and q_v^* is the saturation mass fraction. Therefore, to leading order, the assumption of quasi-steady supersaturation, i.e., $dS/dt = 0$, requires $dq_v/dt = dq_v^*/dt$. Alternatively, we could simply define the quasi-steady approximation as $dq_v/dt = dq_v^*/dt$, which implies that the parcel's mass fraction of water vapor in excess of saturation, $q_v - q_v^*$, is constant in time.

The quasi-steady approximation implies that the rate of actual condensation onto droplets (given by dq_v/dt) matches the rate at which the saturation mass fraction of water vapor changes due to changes in temperature and pressure (given by dq_v^*/dt). The rate dq_v^*/dt depends on the vertical velocity w. The rate dq_v/dt depends on the supersaturation S and the "diameter concentration," which is the sum of droplet diameters per volume (Romps et al. 2023), or, equivalently, the "integral radius," which is the sum of droplet radii per volume (Politovich and Cooper 1988; Korolev and Mazin 2003). We may write the diameter concentration as $n\bar{D}$, where n is the droplet number concentration (with dimensions of inverse volume) and $\bar{D}$ is the mean droplet diameter (with dimensions of length).

Equating dq_v/dt and dq_v^*/dt, we can derive

$$S = F\frac{w}{n\bar{D}}, \tag{1}$$

where F (with dimensions of time per volume) is a function of ambient pressure and temperature. The derivation and full expression for F are given in appendix A. Equation (1) gives the supersaturation to which a parcel will adjust if its $n\bar{D}$ and w remain fixed. That adjustment occurs over a "supersaturation-adjustment time scale" τ_{adjust} [referred to as the "time of phase relaxation" by Korolev and Mazin (2003)], which may be calculated from w and $n\bar{D}$. Therefore, Eq. (1) is a good approximation for the parcel's *current* supersaturation if its w and $n\bar{D}$ have already held steady for much longer than τ_{adjust}. This is expected to be the case for the updrafts studied here, and evidence in support of this is provided by Fig. 2 of Romps et al. (2023), which scatterplots the quasi-steady S against the actual S in cloudy updrafts that have already reached an ascent speed greater than 1 m s^{-1} in a cloud-resolving simulation with spectral-bin microphysics. Similarly, Eq. (1) is a good approximation for the parcel's *future* supersaturation if its w and $n\bar{D}$ will hold steady for much longer than τ_{adjust}. As a corollary to this, expression (1) represents neither the current nor future supersaturation if $n\bar{D}$ is changing rapidly compared to τ_{adjust}, as it will be during periods of rapid activation of aerosols, such as at cloud base or in a newly condensing eddy in the free troposphere.

For back-of-the-envelope calculations, it is fortunate that F varies only weakly with temperature and pressure in the lower tropical troposphere. Figure 1a shows a scatterplot of F versus height above ground level z_{AGL} for all of the 1-Hz samples of pressure, temperature, and height from all of the flights over the Amazon used in this study. Note that F is everywhere between 2 and 3 s m^{-3}. Therefore, we can use $F \approx 2.5$ s m^{-3} with the assurance that this is accurate to within 20%.

To explore the implications of Eq. (1), Fig. 1b plots contours of S on axes of $n\bar{D}$ and w using $F = 2.5$ s m^{-3}. For a given S, $n\bar{D}$ and w are proportional to each other, so isopleths of S appear as straight lines emanating from the origin. We see that, for any updraft speed less than 40 m s^{-1}, a supersaturation of 10% requires a diameter concentration of less than 1 mm cm^{-3}. Likewise, for a more moderate speed of 4 m s^{-1}, a supersaturation of 10% requires a diameter concentration of less than 0.1 mm cm^{-3}. To translate these diameter concentrations to droplet number concentrations, consider a mean droplet diameter $\bar{D}$ of 10 μm. In that case, diameter concentrations of 1 mm cm^{-3} (0.1 mm cm^{-3}) would require a droplet number concentration n of 100 cm^{-3} (10 cm^{-3}). Therefore, as a rule of thumb, we should expect warm-phase invigoration by pollution to be possible only where the droplet number concentration in unpolluted moist convective updrafts is below a threshold of ~10–100 cm^{-3}.

Here, we will be looking at data from the Gulfstream-1 (G-1) aircraft (see section 4), which flew as part of the Observations and Modeling of the Green Ocean Amazon (GoAmazon)

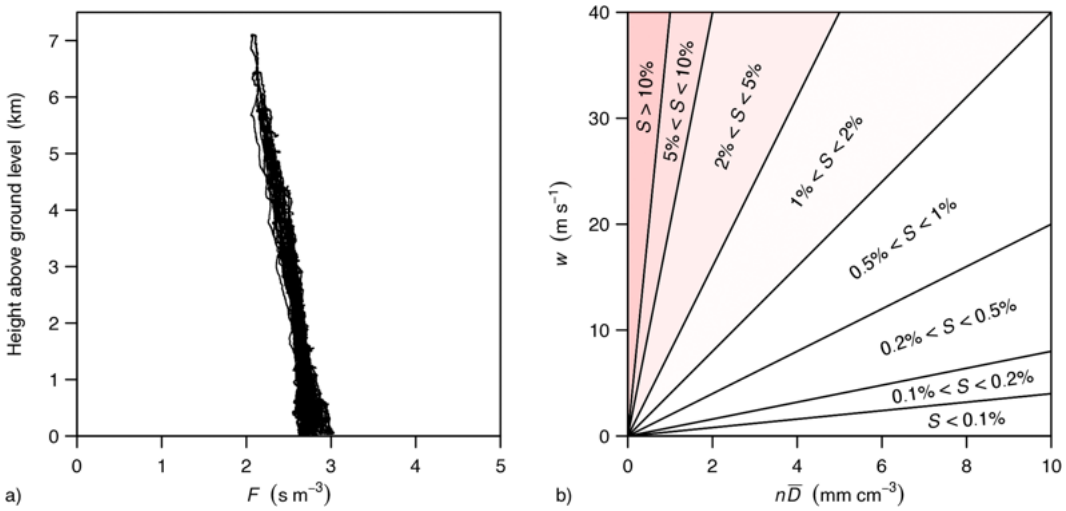

FIG. 1. (a) Values of F, the coefficient in Eq. (1), as calculated from all 1-Hz measurements of ambient pressure and humidity during the GoAmazon G-1 flights. (b) Supersaturation predicted from Eq. (1) as a function of diameter concentration $n\bar{D}$ and vertical velocity w using $F = 2.5$ s m^{-3}. Red color highlights supersaturation values on the order of 10%, which are required for substantial warm-phase invigoration.

campaign during both the 2014 dry season previously analyzed for supersaturation using the High Altitude and Long Range Research (HALO) aircraft by Romps et al. (2023) and the 2014 rainy season (not previously analyzed). Across both seasons, the G-1 spent over 99% of its time in air temperatures greater than 273.15 K and it sampled no air temperatures lower than 267 K; therefore, for all intents and purposes, the aircraft may be considered as having sampled exclusively warm-phase clouds. During the dry-season G-1 flights, the average upwind boundary-layer aerosol concentration was similar to the average value during the HALO flights (1159 cm^{-3} for G-1 vs 1200 cm^{-3} for HALO). Therefore, we may hypothesize that the G-1 aircraft will give values of supersaturation during the dry season similar to those measured with the HALO aircraft, i.e., values of around 0.2% (Romps et al. 2023).

Since supersaturation has not previously been measured for GoAmazon's rainy season, we must turn to a scaling argument to make a hypothesis for the G-1's rainy-season supersaturation values. Romps et al. (2023) derived a $-2/3$ scaling between supersaturation and aerosol number concentration using two assumptions: 1) the number concentration of droplets n is proportional to the number concentration of aerosols n_a and 2) the liquid water content of a cloud ($\sim n\bar{D}^3$) is independent of n_a. Combined, these assumptions give $n\bar{D} \propto n_a^{2/3}$. Substituting into Eq. (1), this gives

$$S \propto w n_a^{-2/3}. \tag{2}$$

While the derivation of Eq. (1) is grounded in fundamental physics (see appendix A), the derivation of Eq. (2) is more heuristic and is likely applicable only across samples of moist convection from similar heights and with similar organization and maturity. This proposed $-2/3$ scaling will be confronted with observational data in section 5. The scaling predicts that the supersaturation measured by the G-1 during the rainy season is only $(328/1159)^{-2/3} = 2.3$ times larger than in the dry season, where 328 and 1159 are the mean number of aerosols, per cubic centimeter, in the boundary layer during the rainy-season and dry-season G-1 flights, respectively. Therefore, this scaling predicts a median rainy-season supersaturation of $2.3 \times 0.2\% \approx 0.5\%$.

3. Method

As noted above, high supersaturation should be expected only when droplet number concentrations are below a threshold of ~10–100 cm^{-3}. But droplet number concentrations lower than these thresholds are extremely common in Earth's atmosphere. Indeed, the vast majority of Earth's atmosphere has a droplet number concentration n of less than 1 cm^{-3}. This does not mean, however, that a supersaturation of 10% is common. Instead, it is important to remember that Eq. (1) is a valid approximation for the actual supersaturation only in cloudy air for which $n\bar{D}$ and w are changing slowly compared to τ_{adjust}. The value of τ_{adjust} is on the order of ~0.1–10 s inside typical warm-phase clouds (Squires 1952; Politovich and Cooper 1988; Korolev and Mazin 2003) but can be much longer at the cloud periphery. Our focus on air within steady moist-convective updrafts means that we are looking inside clouds (not at their periphery) at motions for which the Lagrangian w and $n\bar{D}$ vary on time scales much longer than ~0.1–10 s, thereby ensuring the validity of Eq. (1).

Most past studies (Warner 1968; Politovich and Cooper 1988; Siebert and Shaw 2017) have used qualitative criteria to identify steadily rising cloudy air for the application of Eq. (1). Exceptions to this are Prabha et al. (2011), which required the liquid mass fraction q_c to exceed 0.02 times the adiabatic value, and Romps et al. (2023), which required an air temperature T of >273 K, a liquid mass fraction q_c of $>10^{-4}$, and a vertical velocity w of >1 m s^{-1}. To increase the odds

that we are sampling such steadily rising cloudy air, we will require here that 1) the liquid mass fraction q_c exceeds 10^{-5} (to ensure we are in cloudy air),[1] 2) the height $z_{\rm AGL}$ exceeds 1 km (to exclude cloud-base turbulence), 3) the vertical velocity w exceeds 2 m s^{-1} (to automatically exclude most eddies), and 4) the vertical velocity w exceeds twice the maximum absolute value of vertical velocity in nearby clear air. That fourth condition helps to restrict our application of Eq. (1) to steady-state motions. Note that none of the nearby vertical motion in clear air is in a steady state: at altitudes where we are sampling convective clouds, the atmosphere is stably stratified, so only air with steady condensation or evaporation can be steadily rising or descending, respectively. Therefore, any rising or descending motion in the clear air must be transient. Inside a cloud, there can be steady ascent but also transient vertical motion associated with eddies. To exclude those transient motions, we require that the in-cloud vertical ascent is at least twice as fast as the maximum transient speeds observed in the nearby clear air. The sensitivity of results to these four conditions will be explored in section 5.

4. Data

With the exception of the boundary-layer aerosol concentrations (discussed further below), the data used in this study come from instruments aboard the Department of Energy (DOE) Atmospheric Radiation Measurement (ARM) Aerial Facility (AAF; Schmid et al. 2014) G-1 aircraft. The instruments aboard the G-1 collected data during the GoAmazon 2014/5 campaign (Martin et al. 2016). The flights were conducted during two periods: 16 flights from 22 February to 23 March 2014 (during the rainy season) and 19 flights from 6 September to 4 October 2014 (during the dry season).

The G-1 carried a cloud droplet probe (CDP) manufactured by Droplet Measurement Technologies, which recorded droplet size distributions in 1-μm bins for diameters from 2 to 14 μm and in 2-μm bins from 14 to 50 μm, for a total of 30 bins, reported at 1 Hz. Given the G-1's true airspeed of ~100 m s^{-1}, the analyses performed here will be at a spatial resolution of ~100 m. Two 1-Hz time series are generated from these distributions: the diameter concentration (length per volume) and the liquid water content (LWC; mass per volume). To be precise, define $N(D)$ to be the number of droplets per volume with diameters less than D. The total droplet number concentration n is defined as $n \equiv N(\infty)$. The diameter concentration is then $n\bar{D}$, where $\bar{D}$ is the mean droplet diameter. In particular, the diameter concentration and LWC can be calculated from N as

$$n\bar{D} = \int dD \, \frac{dN}{dD} D, \tag{3}$$

$$\mathrm{LWC} = \int dD \, \frac{dN}{dD} \rho_L \frac{\pi}{6} D^3, \tag{4}$$

where $\rho_L = 10^3$ kg m^{-3} is the density of liquid water.

The G-1 also carried a 20-Hz Aircraft-Integrated Meteorological Measurement System (AIMMS) manufactured by Aventech Research Incorporated. Its data were saved at 1 Hz to files in the IWG1 format, following the standards established by the Interagency Working Group for Airborne Data and Telemetry Systems (IWGADTS). From those files, we obtain $z_{\rm AGL}$ (named Radar_Alt_ft in the data file, calculated from GPS position and altitude using a topographical map), the air pressure p (Static_Press_mbar, from the AIMMS Rosemount 1201F1), the vertical wind speed w (Vert_Wind_Spd_m_s, from the AIMMS), and the air temperature T (Total_Temp_degrees_C, from the AIMMS Rosemount 102E). Periods of obviously bad data were identified by eye and then excluded algorithmically by keeping only those times that satisfy inequalities involving w, $z_{\rm AGL}$, p, and T. Those inequalities exclude spurious vertical velocities and spuriously large departures from a moist adiabat (see appendix B).

Using data from all of the flights combined, the relative data acquisition lag between the CDP and AIMMS instruments is found by calculating the correlation coefficient between the LWC and w time series (interpolated to each other's time values) for all possible lags (at 0.1-s intervals) from −2.5 to +2.5 s and then selecting the lag that gives the highest correlation. This procedure for identifying the relative lag is motivated by the expectation that strong ascent should tend to be collocated with high liquid water. The best fit is found by removing 1.7 s from the times listed in the CDP data files or, equivalently, adding 1.7 s to the times listed in the IWG1 data files. In practice, we remove 1.7 s from the times in the CDP data, generating time-adjusted CDP data that are used henceforth. To treat the CDP and AIMMS data on an equal footing, we interpolate the AIMMS data to the times of the CDP data and vice versa. This effectively doubles the number of observational times, each of which now represents a time interval of 0.5 s. With the CDP and AIMMS datasets synchronized in this way, the condensate mass fraction q_c is calculated as LWC/ρ, where the air density ρ is calculated from the pressure and temperature.

Among all of the G-1 flights, there are 798 s of time when $q_c > 10^{-5}$, $z_{\rm AGL} > 1$ km, and $w > 2$ m s^{-1}, which are three of the four requirements for identifying times when Eq. (1) is applicable. For each such time t, consider the 2-min interval centered on that time, i.e., from $t - 60$ s to $t + 60$ s. If those 2 min (~12 km of flight path) do not contain at least 30 s of w measurements in clear air ($q_c \le 10^{-5}$)—because of instrument error, quality control issues, or being within a nearly uninterrupted cloud layer—then the measurement is discarded. This leaves us with 95% (757.5 s) of the times when $q_c > 10^{-5}$, $z_{\rm AGL} > 1$ km, and $w > 2$ m s^{-1}. We then apply the fourth requirement, which is that $w(t)$ be at least twice the maximum absolute value of vertical velocity measured

[1] It is useful to note that 10^{-5} is a very low threshold for the liquid mass fraction, and so $q_c > 10^{-5}$ is a very liberal definition of cloudy air. To see this, we can calculate the distance h that a saturated cloud must be lifted to increase its liquid mass fraction by 10^{-5}. The relevant equation is $h\gamma q_v^* = 10^{-5}$, where γ is minus the fractional change in q_v^* with height as given by Eq. (6) of Romps (2014). For $T = 280$ K, $\Gamma = 5$ K km^{-1}, and $q_v = 0.01$ (values representative of the tropical lower troposphere), this gives $h = 5$ m, which shows how little ascent is required of a cloud to satisfy $q_c > 10^{-5}$.

in clear air during $t - 60$ s to $t + 60$ s. This gives 129 s of measurements in steady moist-convective updrafts (which we will refer to as simply "updrafts"), during which the supersaturation can be calculated from Eq. (1). Of these 129 s, 41.5 s occur during the rainy season in 15 different cloud transits, with a transit defined as a 2-min interval containing updrafts. Similarly, 87.5 s occur during the dry season in 26 cloud transits.

The G-1 also carried a high-resolution (1080p) forward-looking camera (AXIS P1347 Network Camera). Still frames are gathered for each of the cloud transits when the video was available. Among the 15 rainy-season transits, video is available for 12 of them. To obtain a representative image for each transit, a still frame is taken from the time t when there is a total of 20 s of clear air between t and the time of the transit's first updraft.

For boundary-layer aerosols, data are taken from the Amazon Tall Tower Observatory (ATTO; Andreae et al. 2015), which was the T0a site during GoAmazon (Martin et al. 2016). Among the GoAmazon sites, T0a is the one most reliably upwind of Manaus as it is 150 km to its northeast. For each day with an updraft, the boundary-layer condensation nucleus concentrations from ATTO's condensation particle counter (CPC) are averaged between 1500 and 2000 UTC (the range of times that encompasses all of the updrafts). There are 9 days with updrafts during the rainy season, of which eight have CPC data. There are 12 unique days with updrafts during the dry season, of which 11 have CPC data. The average of the 1500–2000 UTC boundary-layer aerosol number concentration was 328 cm^{-3} on the days of rainy-season updrafts and 1159 cm^{-3} on the days of the dry-season updrafts.

5. Results

The bulk of the results presented here (section 5a) will pertain to moist-convective updrafts defined using the criteria laid out in section 3. For completeness, a brief analysis will also be presented of the supersaturation in all ascending air for which Eq. (1) is likely to be valid (section 5b).

a. Moist-convective updrafts

To begin, we may check whether the G-1's dry-season supersaturation values match the dry-season supersaturation values previously reported by Romps et al. (2023) using the HALO aircraft. From the G-1, we find that the 87.5 s of updrafts during the dry season had a median supersaturation of 0.13% (mean of 0.15%). This is similar to, but somewhat smaller than, the median of ~0.2% found in the same season by the HALO aircraft (Romps et al. 2023).

Of more interest, however, are the values of supersaturation in the rainy season, when aerosol concentrations are lower and, therefore, supersaturation should be higher. During the rainy season, the G-1 measured 41.5 s of updrafts, all of which are shown in context in Fig. 2. This figure shows the time series of vertical velocity (in black) and diameter concentration (in blue) for each of the 15 rainy-season cloud transits. For most transits, an image from the forward camera on the G-1 is shown at the time corresponding to the yellow cross on the abscissa. Note that the ordinate is doing triple duty here: it represents the vertical velocity (in black; for which case the ordinate values represent m s^{-1}), the diameter concentration (in blue; mm cm^{-3}), and the supersaturation (in red; %). As a visual aid, horizontal pink lines are drawn at 0 and 1, and all 41.5 s of supersaturation measurements are shown here as red dots (one for each 0.5 s). Comparing the red dots with the pink reference lines, we see that all of the supersaturation values are $\lesssim$1%. Since higher w favors higher S [see Eq. (1)], it is noteworthy that these updrafts have vertical velocities ranging over ~2–8 m s^{-1}, with a median equal to the 99th percentile of all in-cloud vertical velocities measured by the G-1. Despite looking at the strongest updrafts, the median (mean) of these rainy-season supersaturation values is only 0.46% (0.50%).

As discussed in section 1, we focus here on steady moist-convective updrafts in part because we expect Eq. (1) to be valid within them. To check this, we can calculate the saturation-adjustment length scale $L_{\text{adjust}} \equiv \tau_{\text{adjust}} w$, where the saturation-adjustment time scale τ_{adjust} is defined as in Eq. (17) of Korolev and Mazin (2003). For the 41.5 s of updrafts, the median (mean) value of L_{adjust} is 3 m (3 m), and no value of L_{adjust} exceeds 20 m. These length scales are much shorter than the typical length scale of steady moist-convective updrafts, so it is likely that Eq. (1) is applicable.

Although these measurements were taken over the relatively clean rainy-season Amazon, the supersaturation values are far from the ~10% required for substantial warm-phase invigoration (Fan et al. 2018; Igel and van den Heever 2021; Romps et al. 2023). The reason for this is that the diameter concentrations are high. As discussed in section 2, a cloud ascending at 4 m s^{-1} would need a diameter concentration of 0.1 mm cm^{-3} to generate a supersaturation of 10%. By contrast, the blue curves in Fig. 2 show that the diameter concentrations are 10–20 times higher than that with values of ~1–5 mm cm^{-3} in updrafts. To find $S = 10\%$ with such diameter concentrations, Eq. (1) tells us that we would need to have updraft speeds exceeding 40 m s^{-1}.

To illustrate the variance in the supersaturation measurements, Fig. 3 shows the distributions of the G-1 supersaturation values during the dry season (red) and rainy season (blue). These are normalized distributions presented as the fraction of time per unit interval of $\log_{10}(S)$. It is notable that the dry-season and rainy-season distributions are fairly compact, with each spanning about one order of magnitude from tail to tail. Furthermore, the dry-season value of ~0.2% from the HALO aircraft (Romps et al. 2023) is nearly centered on the distribution of dry-season values from the G-1. All of the observed supersaturation values are smaller than the value needed for substantial warm-phase invigoration (~10%) by about an order of magnitude or more.

To check the scaling proposed by Romps et al. (2023), Fig. 4 plots the mean of each day's supersaturation values (from the G-1) plotted against that day's boundary-layer aerosol number concentration N (from the ATTO CPC), both on log axes. Due to data availability from the ATTO CPC, there are 8 points from the rainy season (blue) and 11 points from the dry season (red). There is no obvious relationship between S and N within an individual season, but, when considered together, there is a statistically significant relationship between $\log(S)$ and $\log(N)$ with a slope of -0.7 [95% confidence interval (CI): from -1.0 to -0.4]. This matches the $-2/3$ slope

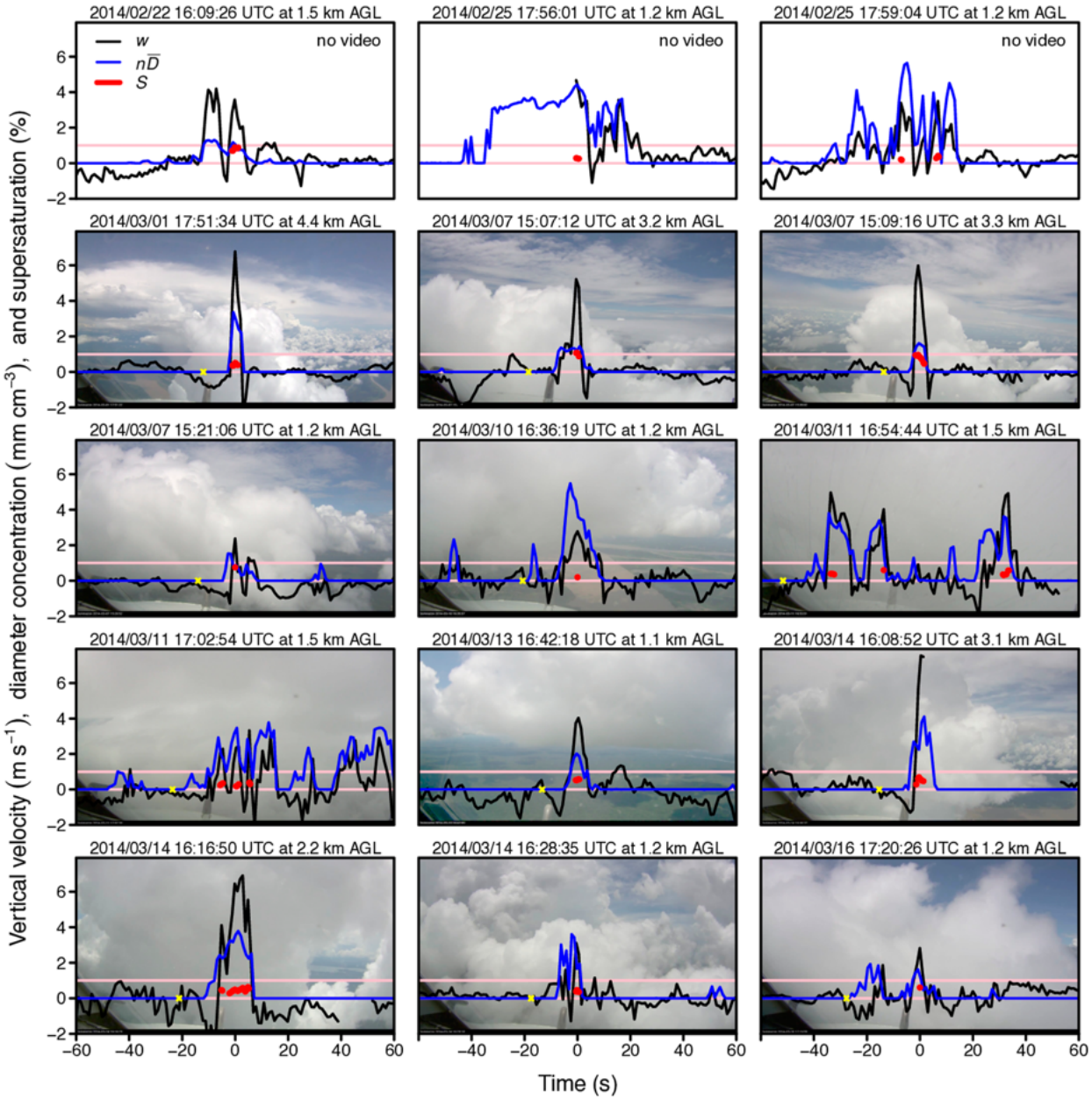

FIG. 2. Observed time series for each of the G-1's 15 cloud transits containing updrafts during the GoAmazon rainy season. Values of the quasi-steady supersaturation (%) calculated from Eq. (1) are shown in red. Also shown are the time series of vertical velocity (black; m s^{-1}) and diameter concentration (blue; mm cm^{-3}). As a visual guide, the horizontal pink lines indicate values of zero and one. When available, an image from the forward camera is shown in the background, taken from the time indicated by the yellow cross on the abscissa. The time on each abscissa is relative to the time given at the top of the panel. The altitude at the top of the panel is the height above ground level of the G-1 at the given time.

expected from the theory of Romps et al. (2023). Since the dry and rainy seasons both have a mean w for their updrafts of 4 m s^{-1}, this difference between seasons is driven by the effect of N on the diameter concentration, not by differences in w. Indeed, regressing $\log(S/w)$ on $\log(N)$ gives the same slope and confidence interval.

Finally, we can test the sensitivity of the calculated supersaturation to the conditions used to identify steadily rising cloudy air. Recall that Eq. (1) is applicable only in steadily rising (and also steadily descending) cloudy air, and that four conditions have been used to restrict to such times: $q_c > 10^{-5}$, $w > 2$ m s^{-1}, $z_{AGL} > 1$ km, and $w > 2|w|_{\text{max-in-clear}}$. The green distribution in Fig. 5 is for all such updraft supersaturation measurements during both the dry and rainy seasons. In other words, it is the time-weighted combination of the two distributions shown in Fig. 3. To illustrate the combinations of vertical

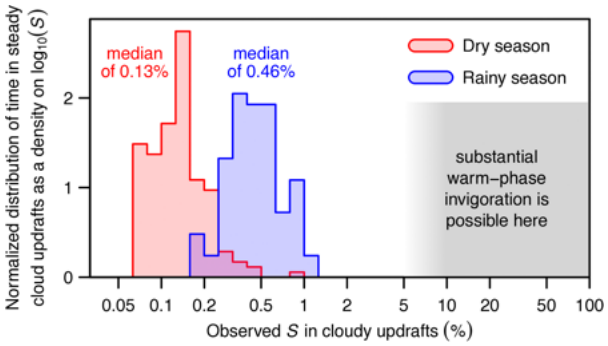

FIG. 3. Normalized distribution of the 87.5 s of dry-season updrafts is shown in red, presented as the fraction of time per unit interval of $\log_{10}(S)$. Note that the interpolation from lag correction has generated 0.5-s intervals from 1-Hz data. The data in blue are similar, but for the 41.5 s during the rainy season.

velocity and diameter concentration that give rise to this distribution of supersaturation, the top-left panel of Fig. 6 shows a scatterplot on w and $n\bar{D}$ of all 258 0.5-s intervals of updrafts (129 s in total). These updrafts have too low a vertical velocity and much too high a diameter concentration to be generating $O(10)$% supersaturation.

The orange distribution in Fig. 5 and orange points in Fig. 6 are generated by removing the minimum thresholds of 2 m s^{-1} and 1 km on vertical velocity and height, respectively. Since the orange distribution still retains the requirement of $w > 2|w|_{\text{max-in-clear}}$, it differs from the green distribution only slightly: there are a few seconds of time added during which Eq. (1) would predict a supersaturation exceeding 1%. Since these seconds of observations are near the cloud base or have

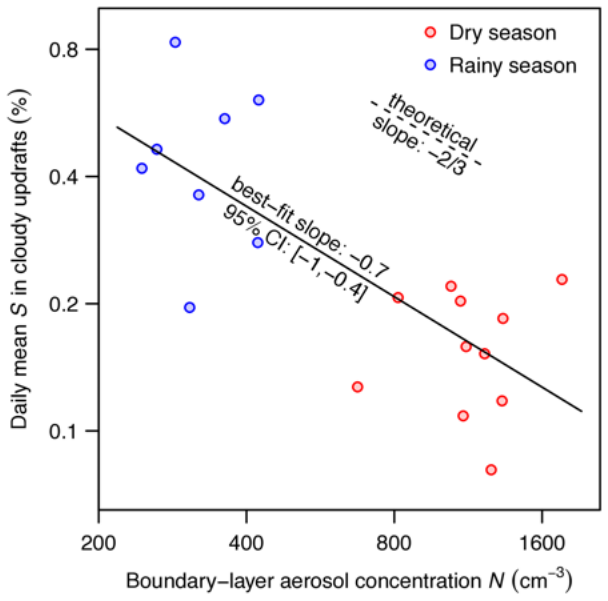

FIG. 4. Daily mean of updraft supersaturation values from 11 dry-season flights (red) and 8 rainy-season flights (blue), plotted against the average boundary-layer aerosol number concentration on those days from 1500 to 2000 UTC.

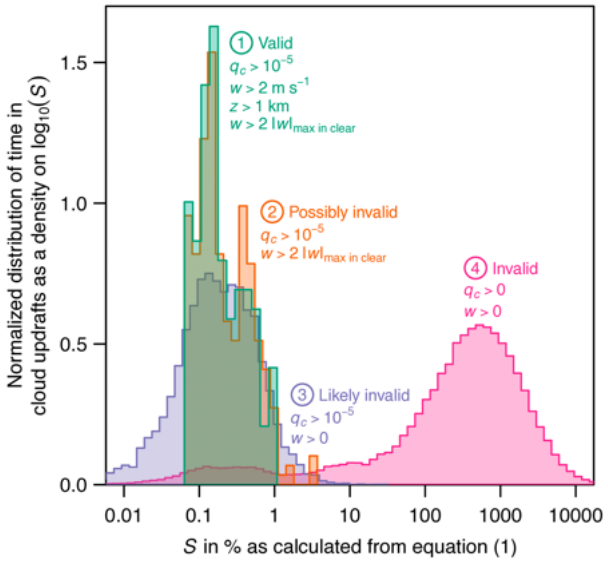

FIG. 5. Normalized distributions of time as a function of supersaturation as calculated from Eq. (1) from all times, i.e., the dry season plus rainy season. Each distribution is for the times when the associated conditions are satisfied. The green color shows times when all four conditions are satisfied: $q_c > 10^{-5}$, $w > 2$ m s^{-1}, $z > 1$ km, and $w > 2|w|_{\text{max-in-clear}}$. The orange color shows times when $q_c > 10^{-5}$ and $w > 2|w|_{\text{max-in-clear}}$ are satisfied. The purple color shows times when $q_c > 10^{-5}$ and $w > 0$ are satisfied. The pink color shows times when $q_c > 0$ and $w > 0$ are satisfied.

small vertical velocities, it is uncertain whether they correspond to steadily rising air. Therefore, we may consider this orange distribution and orange points to contain supersaturation values that are possibly invalid and have labeled them as such. Even if all of these measurements were valid, their small vertical velocities imply that they are relatively uninteresting from the perspective of convective invigoration.

Further relaxing the vertical-velocity condition from $w > 2|w|_{\text{max-in-clear}}$ to $w > 0$, we get the purple distribution in Fig. 5 and purple points in Fig. 6. This purple distribution still mostly overlaps with the green distribution but has a small tail above $S = 1$% and a larger tail extending below $S = 0.1$%. The vast majority of times (about 90%) in these tails have vertical velocities less than 2 m s^{-1}, most of which are not likely associated with steady ascent. Therefore, this collection of supersaturation values is likely invalid. In addition, they have such low vertical velocities that they are largely uninteresting from an invigoration perspective.

If we require only that q_c and w be positive, then we get the pink distribution and pink points, which have very high values of calculated supersaturation. These high values occur because a handful of droplets are very often detected in otherwise clear air. It is important to emphasize that these are invalid values of supersaturation. These values have been calculated with Eq. (1) when Eq. (1) is inapplicable. Only by imposing much more stringent conditions, such as the four conditions used to generate the green distribution, can we have some confidence that Eq. (1) is being applied to steadily rising cloudy air, as is assumed in its derivation.

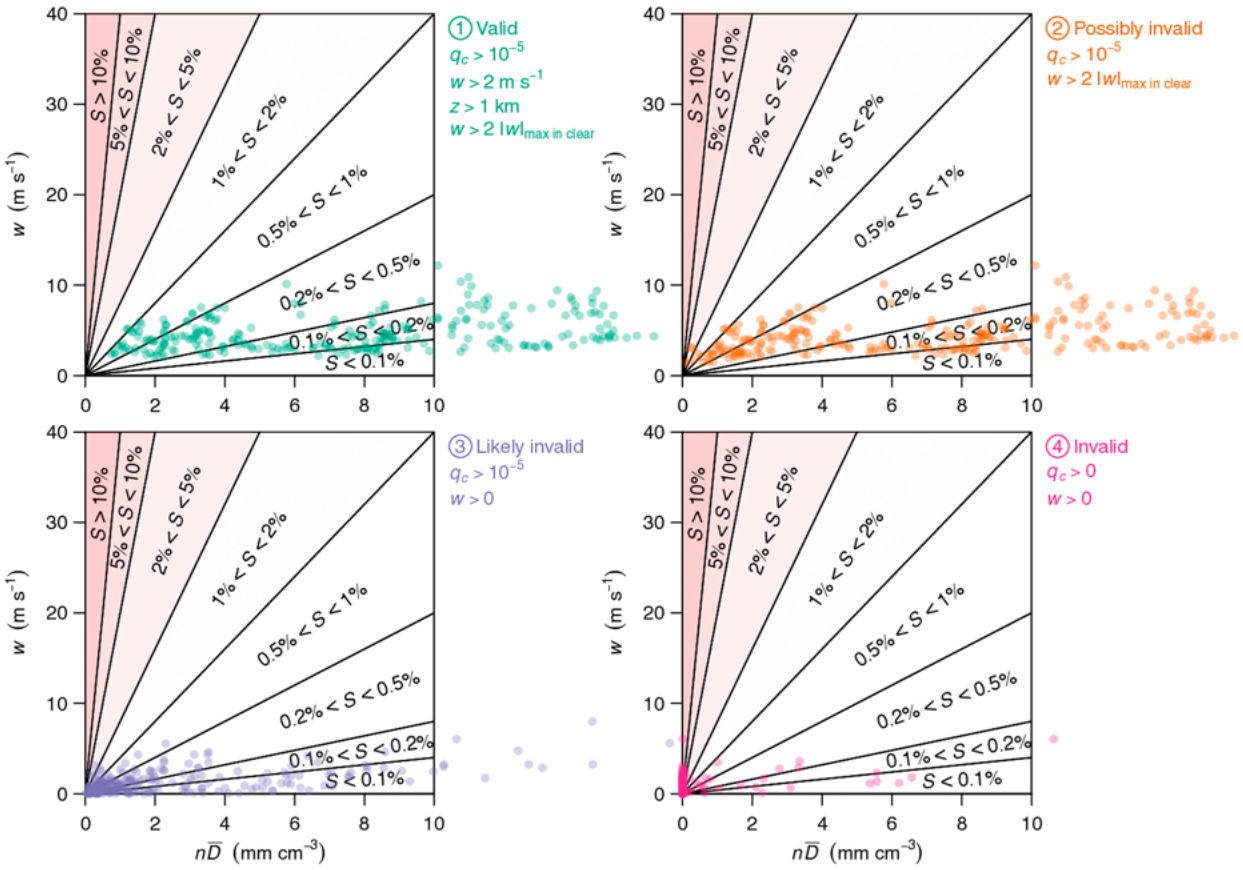

FIG. 6. Scatterplots of vertical velocity vs diameter concentration for the four sets of conditions shown in Fig. 5. For each condition, the points represent 258 0.5-s intervals (129 s in total) sampled randomly without replacement from the total time satisfying the condition.

b. All ascending air

For completeness, we can also look for high supersaturation in all ascending air. To this end, we could try looking at all air with $w > 0$, but this would run into the obvious problem of including dry air. Furthermore, it would include ascending air that is in the process of activating aerosols on a time scale comparable to or shorter than τ_{adjust}, which would make Eq. (1) invalid. Therefore, in addition to $w > 0$, we must also require that the saturation-adjustment length scale L_{adjust} is much smaller than the length scale over which aerosols are typically activated, which is on the order of tens of meters (Howell 1949; Mordy 1959). Therefore, we will restrict ourselves to looking at parcels for which $L_{\text{adjust}} < 10$ m. Across both seasons, there is more than an hour of measurements (4074.5 s) during which the conditions $w > 0$ and $L_{\text{adjust}} < 10$ m are both satisfied. The median (mean) supersaturation during these times is 0.1% (0.2%), and no values are larger than 0.6%. We conclude that, within the limits of applicability of Eq. (1), the values of supersaturation are exclusively low.

6. Summary and discussion

In a search for high supersaturation, we have examined the data collected by the DOE G-1 aircraft during the rainy season of the GoAmazon campaign. To calculate the supersaturation from the available data, we have used the quasi-steady approximation, which allows us to estimate the supersaturation as the updraft speed divided by the droplet diameter concentration times F, which takes values of 2.5 ± 0.5 s m^{-3} (see Fig. 1a). For an updraft speed of 40 m s^{-1} (4 m s^{-1}), a diameter concentration of 1 mm cm^{-3} (0.1 mm cm^{-3}) would be needed to generate a supersaturation of 10% (see Fig. 1b).

Because of their relevance to meteorology in general and to the hypothesis of warm-phase invigoration in particular, we have focused on relatively steady moist-convective updrafts. This focus also provides confidence that Eq. (1) is a valid expression for the supersaturation. To select times with steady in-cloud ascent, the following criteria have been used: a vertical velocity exceeding 2 m s^{-1}, a condensate mass fraction exceeding 10^{-5}, a height above the ground level exceeding 1 km, and a vertical velocity exceeding twice the highest absolute value of clear-air vertical velocity in the surrounding 2-min interval (assuming there is at least 30 s of such time in clear air). Figure 5 explores the consequences of relaxing these conditions.

During the rainy-season flights, there were 41.5 s of observations that met those criteria, which correspond to the times of the red points in Fig. 2. Those red points are the values of

the supersaturation, which all satisfy $S \lesssim 1\%$. In other words, the supersaturation observed in cloudy updrafts during the Amazonian rainy season was all low relative to the ~10% required for substantial warm-phase invigoration (see Fig. 3). The reason for these low values is that the diameter concentration $n\bar{D}$ during those times, as given by the black curve in Fig. 2, is greater than 1 mm cm^{-3} as opposed to being on the order of 0.1 mm cm^{-3}.

As shown in Fig. 4, the supersaturation scales between seasons as the aerosol concentration to the −2/3 power, as predicted by Romps et al. (2023). Given the typical supersaturation of 0.2% observed by Romps et al. (2023) in the polluted dry season, this scaling predicted a typical supersaturation of 0.5% during the rainy season, which is borne out by the observations collected by the G-1 aircraft.

The −2/3 scaling can serve as a guide for when the type of convection sampled during the GoAmazon campaign would be expected to generate supersaturation of ~10%. For S to increase from the observed ~0.5% to ~10% with the same updraft speeds, we would need the aerosol concentrations to decrease from 328 cm^{-3} to $328 \times (10/0.5)^{-3/2}$ cm^{-3} ≈ 4 cm^{-3}. That is far below the typical aerosol concentrations in Earth's marine boundary layer (Heintzenberg et al. 2000).

Out of regard for safety, however, the HALO and G-1 aircraft did not perform a random sampling of moist convection at all heights and stages of development. Although Eq. (2) performs well on the clouds sampled by the HALO and G-1 aircraft, it is likely that including other types and stages of moist convection would break the scaling. For example, the scavenging of droplets by precipitation in more mature stages of moist convection would break the assumed linear relationship between the concentrations of cloud droplets and boundary-layer aerosols. In addition, the dependence of precipitation rates on aerosol concentration would break the assumed invariance of liquid water content.

Although the heuristic Eq. (2) is unlikely to be universal, Eq. (1) stems from basic physics and so applies broadly across all types of steady warm-phase convection. And the predictions of Eq. (1) are clear: For the ~10% supersaturation that would enable substantial warm-phase invigoration, unpolluted clouds must have very high vertical velocities, very low diameter concentrations, or some high/low combination of both (see Fig. 1b).

Acknowledgments. Thanks are due to Fan Mei for help with the observational data and to Adam Varble, Rusen Öktem, and Casey Wall for helpful comments on this manuscript.

Data availability statement. The G-1 CDP data are available at https://iop.archive.arm.gov/arm-iop-file/2014/mao/goamazon/comstock-cdp in files of the form CDP_G1_YYYYMMDDHHMMSS_R2_GoAmazon001s.ict, where YYYY, MM, DD, HH, MM, and SS are the year, month, day, hour, minute, and second, respectively. The G-1 altitude and AIMMS data are available at https://iop.archive.arm.gov/arm-iop-file/2014/mao/goamazon/mei-iwg1 in files of the form aaf.iwg1001s.g1.goamazon.YYYYMMDDa.a2.txt. The G-1 forward-facing video is available at https://iop.archive.arm.gov/arm-iop-file/2014/mao/goamazon/tomlinson-video in files of the form video_G1_YYYYMMDDHHMMSS.mp4 and video_G1_YYYYMMDDHHMMSS.asf. The ATTO CPC data are available in the file at https://ftp.lfa.if.usp.br/ftp/public/LFA_Processed_Data/T0a_ATTO/Level1/T0a_CPC_5219_Level1_30min.csv.

APPENDIX A

The Quasi-Steady Supersaturation

This derivation is reproduced nearly verbatim from Text S5 of Romps et al. (2023), which is covered by the Creative Commons Attribution License. To derive an expression for the quasi-steady supersaturation S, we must first find the following (Squires 1952): 1) the condensation rate c required to keep the supersaturation constant as air ascends at a given speed w and 2) the condensation rate c that occurs in the presence of a given supersaturation S and droplet size distribution. First, the rate of condensation c (dimensions of kg m^{-3} s^{-1}) in an updraft, assuming the relative humidity is near one ($|S| \ll 1$) and constant with height, is $c = -\rho w\, dq_v^*/dz$, where ρ is the air density and q_v^* is the saturation mass fraction of vapor. Using the Clausius–Clapeyron relation and hydrostatic balance, we can derive an expression for c as

$$c = \rho w q_v^* \left(\frac{L\Gamma}{R_v T^2} - \frac{g}{R_a T} \right), \tag{A1}$$

where L is the latent heat of evaporation, Γ is the lapse rate, g is the gravitational acceleration, T is the absolute air temperature, R_a is the specific gas constant of dry air, and R_v is the specific gas constant of water vapor (Romps 2014). On the other hand, given a supersaturation S, a droplet grows by diffusion (of water vapor onto the droplet) and conduction (of released latent heat away from the droplet) at a rate given by

$$\frac{1}{4} D \frac{dD}{dt} = S \left[\left(\frac{L}{R_v T} - 1 \right) \frac{L \rho_L}{k_c T} + \frac{\rho_L R_v T}{k_d p_v^*} \right]^{-1}, \tag{A2}$$

where D is the droplet diameter, ρ_L is the density of liquid water, k_c is the thermal conductivity of air, k_d is the coefficient of diffusion for water vapor in air, and p_v^* is the saturation vapor pressure over liquid (Rogers and Yau 1989). We also know that the condensation is related to the growth of droplets by

$$c = \rho_L \int dD\, \frac{dN}{dD} \frac{\pi}{2} D^2 \frac{dD}{dt}, \tag{A3}$$

where $N(D)$ is the number of droplets per volume with diameters less than D. Combining (A2) and (A3) to eliminate dD/dt, then using Eq. (A1) to eliminate c, and then replacing Γ with the moist adiabatic lapse rate (Romps 2014),

$$\Gamma = \frac{g\left(1 + \dfrac{q_v^* L}{R_a T}\right)}{c_p + \dfrac{q_v^* L^2}{R_v T^2}}, \tag{A4}$$

where c_p is the heat capacity of dry air at constant pressure, we get

$$S = \frac{w}{n\bar{D}} \times \underbrace{\frac{g}{2\pi R_a T}\left[\frac{1}{k_d} + \left(\frac{L}{R_v T} - 1\right)\frac{L p_v^*}{R_v T^2}\frac{1}{k_c}\right]\left(\frac{L R_a}{R_v T} - c_p\right)\left(c_p + \frac{R_a L^2 p_v^*}{R_v^2 T^2 p}\right)^{-1}}_{F}, \tag{A5}$$

where w is the vertical velocity of the air, $n \equiv N(\infty)$ is the total number concentration of cloud droplets, $\bar{D}$ is the mean diameter of the droplets (note that $n\bar{D}$ is the "diameter concentration"), and p is the total air pressure. Equation (A5) is the same as in Paluch and Knight (1984) and Politovich and Cooper (1988) except that here we use $L/R_v T - 1$ instead of $L/R_v T$ (a 5% difference), and Politovich and Cooper (1988) add kinetic factors from Fukuta and Walter (1970). Note that L, p_v^*, k_c, and k_d are temperature dependent and k_d is also pressure dependent. Fitting to empirical data (Rogers and Yau 1989), we parameterize k_c and k_d as

$$k_c = c_1 + c_2 T, \tag{A6}$$

$$k_d = \frac{p_0}{p}(d_1 + d_2 T), \tag{A7}$$

where $c_1 = 2.37 \times 10^{-3}$ J m^{-1} s^{-1} K^{-1}, $c_2 = 7.91 \times 10^{-5}$ J m^{-1} s^{-1} K^{-2}, $d_1 = -1.94 \times 10^{-5}$ m^2 s^{-1}, $d_2 = 1.52 \times 10^{-7}$ m^2 s^{-1} K^{-1}, and $p_0 = 10^5$ Pa. The saturation vapor pressure over liquid (Romps 2017, 2021) is given by

$$p_v^* = p_{v0}^*\left(\frac{T}{T_0}\right)^{(c_{pv} - c_{vl})/R_v} \exp\left[\frac{E_{0v} - (c_{vv} - c_{vl})T_0}{R_v}\left(\frac{1}{T_0} - \frac{1}{T}\right)\right], \tag{A8}$$

where p_{v0}^* is the triple-point pressure, T_0 is the triple-point temperature, c_{pv} is the specific heat capacity of water vapor at constant pressure, c_{vl} is the specific heat capacity of liquid water at constant volume, and E_{0v} is the difference in specific internal energy between water vapor and liquid water at the triple point. Curvature and solute effects modify the equilibrium vapor pressure of droplets by $\lesssim$0.1% for droplets with diameters greater than $\sim$2 μm (Rogers and Yau 1989), and 2 μm is the lower limit of the smallest bin in the CDP dataset, so all droplets contributing to the calculation of the supersaturation in this paper are coming from droplets larger than that size.

APPENDIX B

Exclusion of Bad Data

Obviously bad data from the IWG1 files are identified visually and then are excluded systematically by keeping only those times when all three of the following inequalities are satisfied:

$$|w| < 30 \text{ m s}^{-1}, \tag{B1}$$

$$|z_{\text{AGL}} - (87 \text{ m}) + (8461 \text{ m})\log(p/10^5 \text{Pa})| < 250 \text{ m}, \tag{B2}$$

$$|z_{\text{AGL}} + (T - 300 \text{ K})/(6 \text{ K km}^{-1}) - (1250 \text{ m})| < 2250 \text{ m}. \tag{B3}$$

REFERENCES

Abbott, T. H., and T. W. Cronin, 2021: Aerosol invigoration of atmospheric convection through increases in humidity. *Science*, **371**, 83–85, https://doi.org/10.1126/science.abc5181.

Andreae, M. O., and Coauthors, 2015: The Amazon Tall Tower Observatory (ATTO): Overview of pilot measurements on ecosystem ecology, meteorology, trace gases, and aerosols. *Atmos. Chem. Phys.*, **15**, 10 723–10 776, https://doi.org/10.5194/acp-15-10723-2015.

Cotton, W. R., and R. Walko, 2021: Examination of aerosol-induced convective invigoration using idealized simulations. *J. Atmos. Sci.*, **78**, 287–298, https://doi.org/10.1175/JAS-D-20-0023.1.

Dagan, G., P. Stier, G. Spill, R. Herbert, M. Heikenfeld, S. C. van den Heever, and P. J. Marinescu, 2022: Boundary conditions representation can determine simulated aerosol effects on convective cloud fields. *Commun. Earth Environ.*, **3**, 71, https://doi.org/10.1038/s43247-022-00399-5.

Ditas, F., R. A. Shaw, H. Siebert, M. Simmel, B. Wehner, and A. Wiedensohler, 2012: Aerosols-cloud microphysics-thermodynamics-turbulence: Evaluating supersaturation in a marine stratocumulus cloud. *Atmos. Chem. Phys.*, **12**, 2459–2468, https://doi.org/10.5194/acp-12-2459-2012.

Fan, J., and Coauthors, 2018: Substantial convection and precipitation enhancements by ultrafine aerosol particles. *Science*, **359**, 411–418, https://doi.org/10.1126/science.aan8461.

Fujiwara, M., M. Shiotani, F. Hasebe, H. Vömel, S. J. Oltmans, P. W. Ruppert, T. Horinouchi, and T. Tsuda, 2003: Performance of the Meteolabor "Snow White" chilled-mirror hygrometer in the tropical troposphere: Comparisons with the Vaisala RS80 A/H-Humicap sensors. *J. Atmos. Oceanic Technol.*, **20**, 1534–1542, https://doi.org/10.1175/1520-0426(2003)020<1534:POTMSW>2.0.CO;2.

Fukuta, N., and L. A. Walter, 1970: Kinetics of hydrometeor growth from a vapor-spherical model. *J. Atmos. Sci.*, **27**, 1160–1172, https://doi.org/10.1175/1520-0469(1970)027<1160:KOHGFA>2.0.CO;2.

Heintzenberg, J., D. C. Covert, and R. V. Dingenen, 2000: Size distribution and chemical composition of marine aerosols: A compilation and review. *Tellus*, **52B**, 1104–1122, https://doi.org/10.3402/tellusb.v52i4.17090.

Howell, W. E., 1949: The growth of cloud drops in uniformly cooled air. *J. Meteor.*, **6**, 134–149, https://doi.org/10.1175/1520-0469(1949)006<0134:TGOCDI>2.0.CO;2.

Igel, A. L., and S. C. van den Heever, 2021: Invigoration or enervation of convective clouds by aerosols? *Geophys. Res. Lett.*, **48**, e2021GL093804, https://doi.org/10.1029/2021GL093804.

Koren, I., G. Dagan, and O. Altaratz, 2014: From aerosol-limited to invigoration of warm convective clouds. *Science*, **344**, 1143–1146, https://doi.org/10.1126/science.1252595.

Korolev, A. V., and I. P. Mazin, 2003: Supersaturation of water vapor in clouds. *J. Atmos. Sci.*, **60**, 2957–2974, https://doi.org/10.1175/1520-0469(2003)060<2957:SOWVIC>2.0.CO;2.

Martin, S. T., and Coauthors, 2016: Introduction: Observations and modeling of the Green Ocean Amazon (GoAmazon2014/5).

Atmos. Chem. Phys., **16**, 4785–4797, https://doi.org/10.5194/acp-16-4785-2016.

Mordy, W., 1959: Computations of the growth by condensation of a population of cloud droplets. *Tellus*, **11A**, 16–44, https://doi.org/10.1111/j.2153-3490.1959.tb00003.x.

Öktem, R., D. M. Romps, and A. C. Varble, 2023: No warm-phase invigoration of convection detected during GoAmazon. *J. Atmos. Sci.*, **80**, 2345–2364, https://doi.org/10.1175/JAS-D-22-0241.1.

Paluch, I. R., and C. A. Knight, 1984: Mixing and the evolution of cloud droplet size spectra in a vigorous continental cumulus. *J. Atmos. Sci.*, **41**, 1801–1815, https://doi.org/10.1175/1520-0469(1984)041<1801:MATEOC>2.0.CO;2.

Peters, J. M., Z. J. Lebo, D. R. Chavas, and C.-Y. Su, 2023: Entrainment makes pollution more likely to weaken deep convective updrafts than invigorate them. *Geophys. Res. Lett.*, **50**, e2023GL103314, https://doi.org/10.1029/2023GL103314.

Politovich, M. K., and W. A. Cooper, 1988: Variability of the supersaturation in cumulus clouds. *J. Atmos. Sci.*, **45**, 1651–1664, https://doi.org/10.1175/1520-0469(1988)045<1651:VOTSIC>2.0.CO;2.

Prabha, T. V., A. Khain, R. S. Maheshkumar, G. Pandithurai, J. R. Kulkarni, M. Konwar, and B. N. Goswami, 2011: Microphysics of premonsoon and monsoon clouds as seen from in situ measurements during the Cloud Aerosol Interaction and Precipitation Enhancement Experiment (CAIPEEX). *J. Atmos. Sci.*, **68**, 1882–1901, https://doi.org/10.1175/2011JAS3707.1.

Raymond, D. J., and X. Zeng, 2005: Modelling tropical atmospheric convection in the context of the weak temperature gradient approximation. *Quart. J. Roy. Meteor. Soc.*, **131**, 1301–1320, https://doi.org/10.1256/qj.03.97.

Rogers, R. R., and M. K. Yau, 1989: *A Short Course in Cloud Physics*. 3rd ed. Butterworth-Heinemann, 290 pp.

Romps, D. M., 2014: An analytical model for tropical relative humidity. *J. Climate*, **27**, 7432–7449, https://doi.org/10.1175/JCLI-D-14-00255.1.

——, 2017: Exact expression for the lifting condensation level. *J. Atmos. Sci.*, **74**, 3891–3900, https://doi.org/10.1175/JAS-D-17-0102.1.

——, 2021: The Rankine–Kirchhoff approximations for moist thermodynamics. *Quart. J. Roy. Meteor. Soc.*, **147**, 3493–3497, https://doi.org/10.1002/qj.4154.

——, K. Latimer, Q. Zhu, T. Jurkat-Witschas, C. Mahnke, T. Prabhakaran, R. Weigel, and M. Wendisch, 2023: Air pollution unable to intensify storms via warm-phase invigoration. *Geophys. Res. Lett.*, **50**, e2022GL100409, https://doi.org/10.1029/2022GL100409.

Rosenfeld, D., U. Lohmann, G. B. Raga, C. D. O'Dowd, M. Kulmala, S. Fuzzi, A. Reissell, and M. O. Andreae, 2008: Flood or drought: How do aerosols affect precipitation? *Science*, **321**, 1309–1313, https://doi.org/10.1126/science.1160606.

Saleeby, S. M., S. R. Herbener, S. C. van den Heever, and T. L'Ecuyer, 2015: Impacts of cloud droplet–Nucleating aerosols on shallow tropical convection. *J. Atmos. Sci.*, **72**, 1369–1385, https://doi.org/10.1175/JAS-D-14-0153.1.

Schmid, B., and Coauthors, 2014: The DOE ARM aerial facility. *Bull. Amer. Meteor. Soc.*, **95**, 723–742, https://doi.org/10.1175/BAMS-D-13-00040.1.

Schumacher, C., and R. Houze Jr., 2003: Stratiform rain in the tropics as seen by the TRMM precipitation radar. *J. Climate*, **16**, 1739–1756, https://doi.org/10.1175/1520-0442(2003)016<1739:SRITTA>2.0.CO;2.

——, and A. Funk, 2023: Assessing convective-stratiform precipitation regimes in the tropics and extratropics with the GPM satellite radar. *Geophys. Res. Lett.*, **50**, e2023GL102786, https://doi.org/10.1029/2023GL102786.

Seiki, T., and T. Nakajima, 2014: Aerosol effects of the condensation process on a convective cloud simulation. *J. Atmos. Sci.*, **71**, 833–853, https://doi.org/10.1175/JAS-D-12-0195.1.

Sheffield, A. M., S. M. Saleeby, and S. C. van den Heever, 2015: Aerosol-induced mechanisms for cumulus congestus growth. *J. Geophys. Res. Atmos.*, **120**, 8941–8952, https://doi.org/10.1002/2015JD023743.

Shen, C., C. Zhao, N. Ma, J. Tao, G. Zhao, Y. Yu, and Y. Kuang, 2018: Method to estimate water vapor supersaturation in the ambient activation process using aerosol and droplet measurement data. *J. Geophys. Res. Atmos.*, **123**, 10 606–10 619, https://doi.org/10.1029/2018JD028315.

Siebert, H., and R. A. Shaw, 2017: Supersaturation fluctuations during the early stage of cumulus formation. *J. Atmos. Sci.*, **74**, 975–988, https://doi.org/10.1175/JAS-D-16-0115.1.

Sobel, A. H., and C. S. Bretherton, 2000: Modeling tropical precipitation in a single column. *J. Climate*, **13**, 4378–4392, https://doi.org/10.1175/1520-0442(2000)013<4378:MTPIAS>2.0.CO;2.

Squires, P., 1952: The growth of cloud drops by condensation. I. General characteristics. *Aust. J. Sci. Res.*, **5**, 59–86, https://doi.org/10.1071/CH9520059.

Stier, P., and Coauthors, 2024: Multifaceted aerosol effects on precipitation. *Nat. Geosci.*, **17**, 719–732, https://doi.org/10.1038/s41561-024-01482-6.

Varble, A. C., A. L. Igel, H. Morrison, W. W. Grabowski, and Z. J. Lebo, 2023: Opinion: A critical evaluation of the evidence for aerosol invigoration of deep convection. *Atmos. Chem. Phys.*, **23**, 13 791–13 808, https://doi.org/10.5194/acp-23-13791-2023.

Warner, J., 1968: The supersaturation in natural clouds. *J. Rech. Atmos.*, **3**, 233–237.

Yeom, J. M., S. S. Yum, F. Mei, B. Schmid, J. Comstock, L. A. T. Machado, and M. A. Cecchini, 2019: Impact of secondary droplet activation on the contrasting cloud microphysical relationships during the wet and dry seasons in the Amazon. *Atmos. Res.*, **230**, 104648, https://doi.org/10.1016/j.atmosres.2019.104648.